Preparation and Field-Emission of TaSe₂ Nanobelt Quasi-Arrays, and Electrical Transport of Its Individual Nanobelt

Xingcai Wu[1,*], Yourong Tao[1], Liang Li[2], Tianyou Zhai[2,*],
Yoshio Bando[2], and Dmitri Golberg[2]

[1] *Key Laboratory of Mesoscopic Chemistry of MOE, and School of Chemistry and Chemical Engineering,*
Nanjing University, Nanjing 210093, China
[2] *International Center for Young Scientists (ICYS) and International Center for Materials Nanoarchitectonics (MANA),*
National Institute for Materials Science (NIMS), Namiki 1-1, Tsukuba, Ibaraki 305-0044, Japan

3R-TaSe₂ nanobelt quasi-arrays were gown on a Ta foil by a facile two-step method, namely, firstly the TaSe₃ nanobelt arrays were grown on a Ta foil by a surface-assisted chemical vapor transport, and then they were pyrolyzed to 3R-TaSe₂ nanobelt quasi-arrays in vacuum. The nanobelts have low work function and the Ta foil has high conductivity, so the nanobelt arrays possess good electronic field emission performance with a low turn-on (3.6 V/μm) and threshold fields (4.3 V/μm) (which are defined as the macroscopic field required to produce a current density of 10 μA/cm² and 1 mA/cm², respectively) and a high enhancement factor (1045) at an emission distance of 200 μm. The electric transport of the individual nanobelt reveals that it is a high-conductive semiconductor, and observed by the variable-range hopping model. It suggests that the nanobelts have potential applications in field emission and field effect transistors.

Keywords: Tantalum Diselenide, Nanobelt Quasi-Arrays, Field Emission, Electric Transport.

1. INTRODUCTION

One-dimensional (1D) nanostructures have attracted considerable attention due to their unique physical properties caused by quantum size effects and potential applications in nanoscale electronic and optoelectronic devices.[1–6] Based on quantum size effects field effect transistors (FETs) made of individual nanowires,[7–10] and electronic field-emission (FE) prototype devices composed of aligned nanowires[11–13] have been fabricated. To meet different demands it is very important to develop novel 1D nanostructures and investigate their physical properties. Tantalum diselenide (TaSe₂) is a layered inorganic electric conductor (work function: 5.4 eV)[14] and its crystal adopts various polymorphic forms depending on the coordination of metal atoms such as 1T-, 2Ha-, 4Hb-, 4Hc-, 3R- and 6R-TaSe₂. These forms show different physical properties, for example, 1T-TaSe₂ possesses diamagnetic and semiconducting bebaviors while the other forms reveal nearly temperature-independent paramagnetism. and

metallicity.[15,16] 2H-TaSe₂ reveals two charge density wave (CDW) phase transitions: an incommensurate triple one at $T_{ICDW} = 122$ K and a first-order lock-in transition to a commensurate phase at $T_{CDW} = 90$ K.[17] Over the last several decades, TaSe₂ powders,[18] crystals,[19,20] films,[16] nanocrystals,[21,22] and intercalation compounds,[23] as well as NbSe₃, NbSe₂, and TaSe₃ nanobelts,[24–27] have been synthesized, but TaSe₂ nanobelts (or nanowires) have not been reported to date, because their synthesis is still a challenge. The present authors have tried to prepare 1D nanostructures of TaSe₂ by a surface-assisted chemical vapor transport (SACVT) reaction of Se powders and Ta foils (one-step method), however, only TaSe₃ nanobelt arrays have been obtained. Because TaSe₂ has low work function and good conductivity, if its nanobelts arrays are directly grown on a metal substrate, the FE properties can remarkably be improved due to the strong local electric field at the belt tips and low contact resistance between nanobelts and a substrate.[28–37] Here we synthesized quasi-aligned 3R-TaSe₂ nanobelts on a Ta foil by a two-step method.[38,39] Firstly, the TaSe₃ nanobelt arrays were grown on a Ta foil by a SACVT, and then the precursors were

---

*Authors to whom correspondence should be addressed.

RESEARCH ARTICLE

pyrolyzed to align TaSe$_2$ nanobelts in vacuum. The field emission measurements showed that the arrays could be decent field emitters with a low turn-on (3.6 V/μm) and threshold (4.3 V/μm) fields and a high enhancement factor (1045) at an emission distance of 200 μm. To understand the basic physical properties of the nanobelts, the electric transport performance of a single TaSe$_2$ nanobelt has been investigated.

2. EXPERIMENTAL DETAILS

2.1. Preparation of Aligned TaSe$_3$ Nanobelts

673.5 mg of Tantalum (Ta) foils (99.9%, $35 \times 5 \times 0.2$ mm^3) and 146.8 mg of Selenium (Se) powders (99.9%) (molecular ratio of Ta/Se of 1:0.5) were sealed in a quartz ampoule (Φ6 mm $\times$ 10 cm) under vacuum (ca. 10^{-2} Pa). The Ta foils were put at the center section of the ampule. Then the ampoule was placed at the center of a conventional horizontal furnace (Φ4 cm $\times$ 32 cm) with a temperature gradient of ca. 10 Kcm^{-1} from the center to edge. The furnace was heated to 550 °C at a rate of 10 °C/min and kept at this temperature for 6 h. Then the furnace was naturally cooled to room temperature and the Ta foils with the TaSe$_3$ nanobelt arrays were extracted.

2.2. Preparation of Aligned TaSe$_2$ Nanobelts

The foils with the TaSe$_3$ nanobelts were again sealed in another quartz ampoule under vacuum (Φ6 mm $\times$ 30 cm, ca. 10^{-2} Pa). Then one end of the quartz ampoule with the TaSe$_3$ nanobelt arrays was again placed at the center of the horizontal furnace (Φ4 cm $\times$ 32 cm), and remained there at 750 °C for 1.5 h, while the other end was extended about 10 cm outside of the furnace so that the thermolyzed selenium was deposited on the cold end. After the reaction finished and the ampoule cooled to room temperature the foils with TaSe$_2$ nanobelt arrays were extracted from the ampule.

2.3. Characterization

The products were characterized by an X-ray diffractometer (XRD) under monochromatized Cu Kα1-radiation (Shimadzu XRD-6000), a LEO-1530VP scanning electron microscope (SEM) with an energy dispersive X-ray spectrometer (EDX), a JEOL-JEM-2010 high-resolution electron microscope (HRTEM) using imaging and selected area electron diffraction (SAED). Field-emission properties were measured at room-temperature in a high vacuum chamber at a pressure of 2.2×10^{-6} Pa. A rod-like copper probe with a cross section of 1 mm^2 was used as an anode and an aligned TaSe$_2$ nanobelt film served as a cathode. A dc voltage sweeping from 100 to 1100 V was applied to the samples.

2.4. Device Fabrication and Characterization

For FET device fabrication TaSe$_2$ nanobelts were suspended in ethanol by a brief sonication and then deposited on an oxidized Si wafer substrate with a 200 nm thick thermal oxide layer that serves as a gate oxide. The standard photolithography technique followed by Cr/Au (10 nm/100 nm) metal evaporation and a lift-off procedure were used to define the source and drain electrodes, and to electrically contact TaSe$_2$ nanobelts. The current–voltage (I–V) characteristics were recorded at room (HiSOL, Inc) and low temperature (Nagase Electronic Equipments service, co.) using probing systems and a semiconductor parameter analyzer (Keithley Instruments Inc).

3. RESULTS AND DISCUSSION

3.1. TaSe$_3$ and TaSe$_2$ Nanobelt Arrays

The structure of the as-grown products has been determined by X-ray diffraction (XRD). As shown in Figure 1(a), the nanobelt arrays synthesized in first step can be indexed as a monoclinic TaSe$_3$ phase (S.G. P2$_1$/m, $a = 10.41$ Å, $b = 3.494$ Å, $c = 9.836$ Å, $\beta = 106.4°$; JCPDS File 18-1310). After the TaSe$_3$ nanobelt arrays are thermally decomposed in vacuum, the products crystallize in a hexagonal 3R-TaSe$_2$ phase (S.G. R3m, $a = 3.434$ Å, $c = 19.17$ Å; JCPDS File 73-1800) (Fig. 1(b)). The nanobelt morphologies were investigated by scanning electron microscopy (SEM). Figure 1(c) is a plan-view SEM image of aligned TaSe$_3$ nanobelts on a Ta foil, showing that the TaSe$_3$ nanobelts are grown on the large-area of the foil. Figure 1(d) is a side-view SEM image of the aligned TaSe$_3$ nanobelts, revealing that the nanobelts grew almost vertically, and a length of the nanobelts is up to 23 μm. Figure 1(e) is a high-magnification SEM image of the nanobelts, showing that the nanostructures are really in belt-like morphologies, the size is uniform, and a typical nanobelt has a rectangular section of $\sim$40 $\times$ 200 nm^2. High-resolution electron microscopy (HRTEM) image (Fig. 1(f)) of a single nanobelt and corresponding fast Fourier transform (FFT) (inset) demonstrate that the nanobelt grew along the [010] direction. Lattice fringe spacing of 0.94 nm corresponds to the (001) plane of a monoclinic TaSe$_3$ (JCPDS File 18-1310). A nanobelt configuration is drawn in the inset of Figure 1(e). An energy-dispersive X-ray spectrum of the nanobelts displays the coexistence of Ta and Se, and the elemental atomic ratio is 2.94, close to the 1:3.0 stoichiometry, as expected (Fig. 1(f)).

Figure 2(a) shows the XRD pattern of the TaSe$_2$ nanobelts quasi-arrays. Figures 2(b)–(d) are the low-magnification side-view, low-magnification plan-view, and high-magnification plan-view SEM images of the nanobelts arrays, respectively, revealing that the size of

the nanobelts is close to precursors. A transmission electron microscopy (TEM) image and selected area electron diffraction (SAED) pattern (inset) (Fig. 2(e)) of an individual nanobelt show that it grew along the [110] direction. The nanobelt configuration is presented in the inset of Figure 2(e). Figures 2(f) and (g) show chemical mappings of Se and Ta species, respectively, further confirming the coexistence of the Ta and Se atoms. EDX spectrum reveals the presence of Ta and Se at the atomic ratio of 1:2.01, close to the 1:2.0 stoichiometry, as expected (Fig. 2(h)). The growth of TaSe$_3$ nanobelts may be explained by a modified vapor–solid growth mechanism because no droplets are observed on the nanobelt ends.[38] First, Se is evaporated and transported onto the surface of the Ta foils, reacting with a Se vapor (boiling point: 684.9 °C) to form a TaSe$_3$ seed layer on the surface of the foils. As the reaction proceeds, TaSe$_3$ molecules in a gas phase continuously deposit on the seeds to form nanobelts because the seeds induce. The reaction is Ta + 3Se = TaSe$_3$. TaSe$_3$

nanobelts quasi-arrays are converted into TaSe$_2$ nanobelts quasi-arrays because of thermal decomposition of TaSe$_3$ nanobelts quasi-arrays in vacuum. Se is deposited on the cool end of the quartz ampoule extended outside the furnace because Se is vapored. The products are confirmed by XRD, so the reactions can be written as TaSe$_3$ = TaSe$_2$ + Se (vapor).

3.2. Electronic Field Emission Properties of 3R-TaSe$_2$ Nanobelt Arrays

The TaSe$_2$ nanobelt arrays are ideal objects for electron FE. Figure 3(a) depicts the curve of the J versus E measured at an emission distance of 200 μm and a 100–1100 V bias voltage range, and the inset shows the corresponding plots of Ln (J/E^2) versus $1/E$. Based on the J–E curves, we determine the nanobelt field emission turn-on and threshold fields, which are respectively defined as the macroscopic field required to produce a
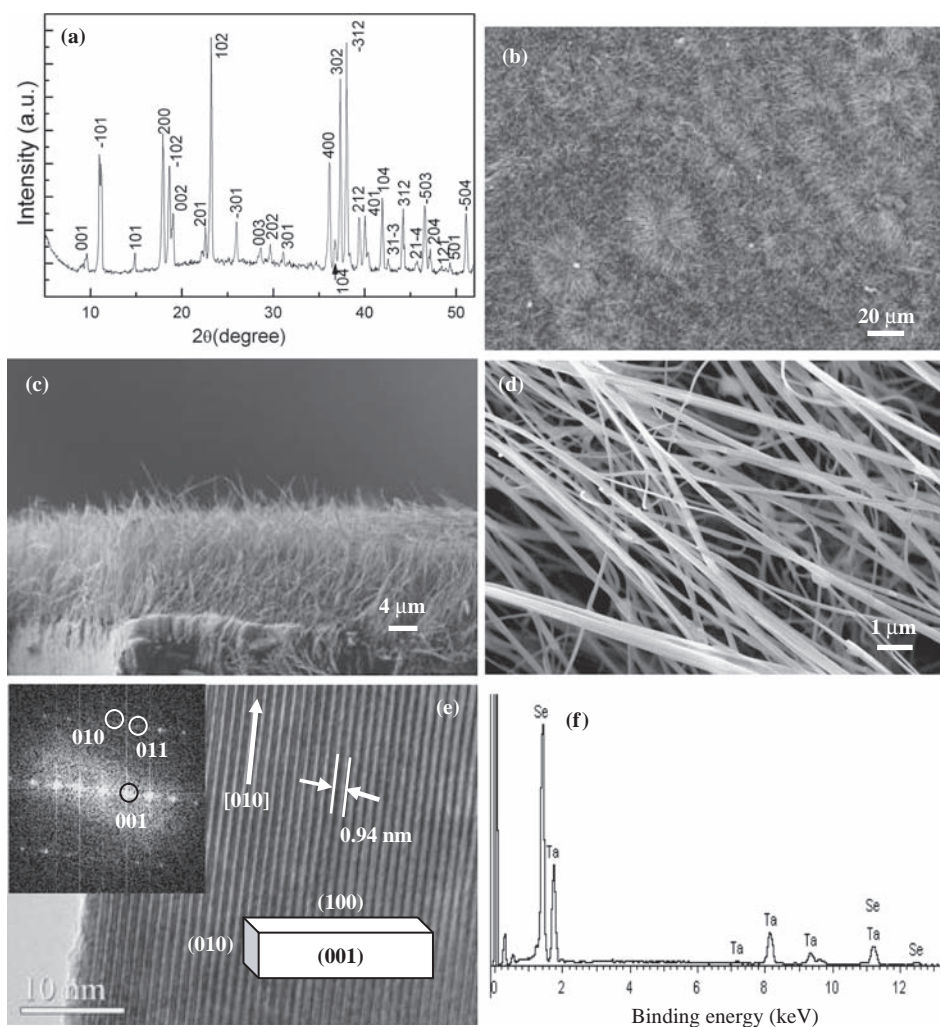
Fig. 1. (a) XRD patterns of TaSe$_3$ nanobelts scraped off Ta foil. (b) Low-magnification plan-view, (c) low-magnification side-view, and (d) high-magnification side-view SEM images of quasi-aligned TaSe$_3$ nanobelts grown on a Ta foil. (e) HRTEM image, fast Fourier transition patterns (inset, left above), and nanobelt configuration (inset, right down) of a single nanobelt. (f) EDX spectrum of TaSe$_3$ nanobelts.
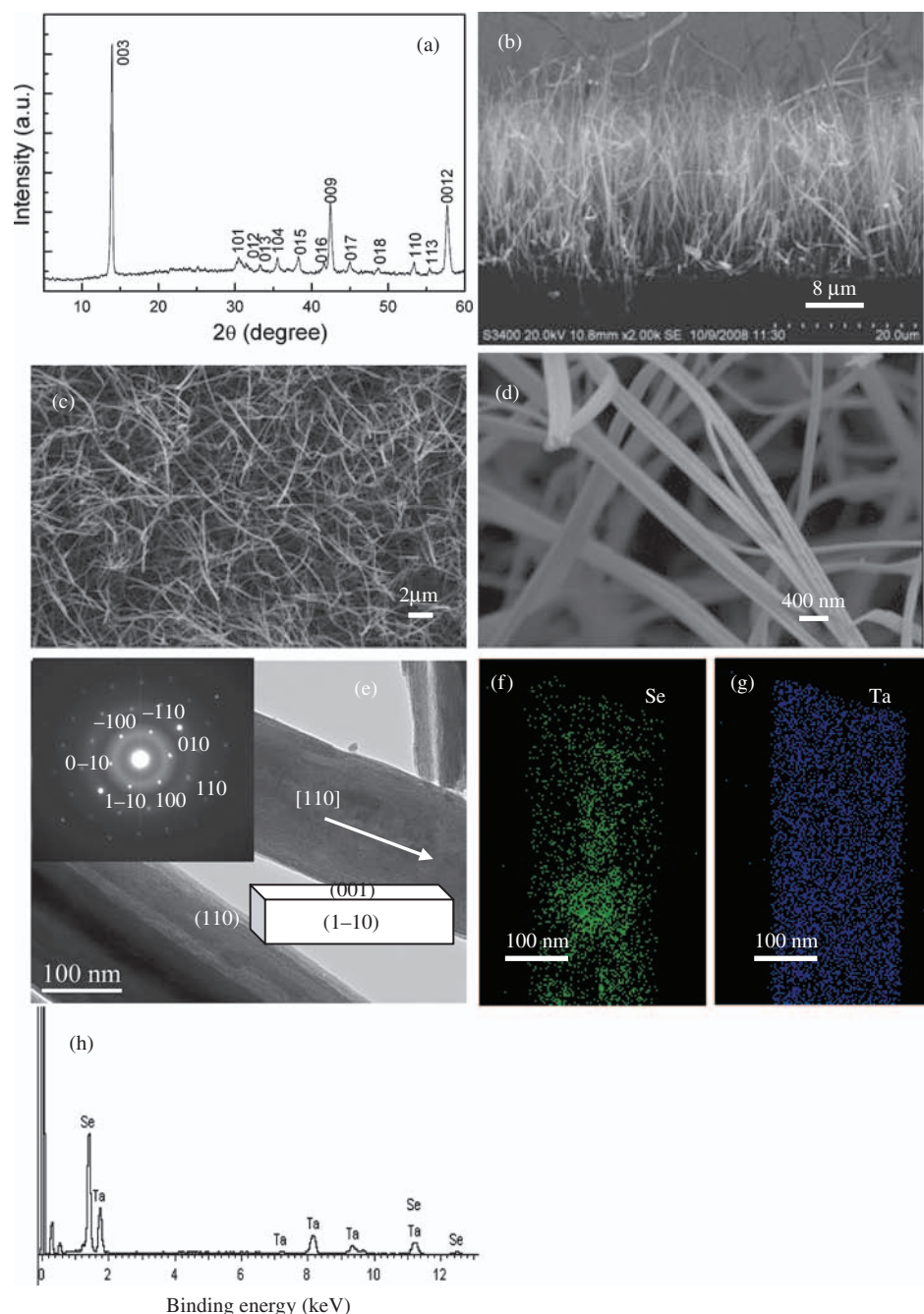
Fig. 2. (a) XRD patterns of TaSe₂ nanobelts scraped off Ta foil. (b) Low-magnification side-view, (c) low-magnification plan-view, and (d) high-magnification plan-view SEM images of quasi-aligned TaSe₂ nanobelts on a Ta foil. (e) TEM image and SAED pattern (inset) of a single nanobelt. (f) Chemical mapping of Se species. (g) Chemical mapping of Ta species. (h) EDX spectrum of TaSe₂ nanobelts.

current density of 10 μA/cm² and 1 mA/cm², as 3.6 and 4.3 V/μm, respectively, whereas maximum emission current density is 5.39 mA/cm² (applied field: 5.49 V/μm). The values are comparable or even surpass those mentioned in the previous reports on ZnO, ZnS, CdS, Si, AlN, NbSe₂, NbN nanowires/nanobelts quasi-arrays.[40–43] The emission current–voltage characteristics were analyzed by the Fowler—Nordheim (FN) equation for the field emission: $J = (AE^2\beta^2/\Phi)\exp[-B\Phi^{3/2}/(E\beta)]$, where J is the

current density (A/m²), E is the applied field, $B = 6.83 \times 10^9$ (eV$^{-3/2}$Vm^{-1}), $A = 1.56 \times 10^{-10}$ (AV^{-2} eV), β is a field enhancement factor, Φ is the work function.[44] The FN plots exhibit an approximately linear behavior in the high field region indicating that electronic emission follows the FN mechanism. The slight bias of linearity may be ascribed to space charge effects in the vacuum space.[45] By determining the slope of the Ln (J/E^2) versus $1/E$ plot using the work function value of TaSe₂ (5.4 eV),

4

the field-enhancement factor, β, has been calculated to be about 1045. Generally, FE performance is dependent on the geometrical features of the emitters, the spatial distribution of emitting centers,[46, 47] and substrate resistance, so the efficient electron FE of the aligned TaSe$_2$ nanobelts has mainly been attributed to their small thickness, and low-resistance of metal substrates. In order to fully understand the electronic FE performance of the nanobelt arrays, FE measurements under changing the anode–cathode distance have been carried out. When the emission distance of the nanobelts arrays changes to 120 μm, the turn-on and threshold fields become 5.6 and 6.6 V/μm, respectively, maximum emission current density is up to 24.4 mA/cm^2 (applied field: 9.2 V/μm), and β is ca.594 (Fig. 3(b)). It further confirms that the present nanobelt arrays are excellent field emitters. Stability of the field-emitters is another important parameter related to potential applications. Field emission stability measurements on the TaSe$_2$ nanobelt arrays were performed by keeping an electric field at 7.7 V/μm over a period of 5.6 hours. As shown in Figure 3(c), there were no current degradations or notable fluctuations during this period. It indicates that the nanostructures have potential applications in the cold-cathode-based electronics. In addition, the FE properties of the TaSe$_3$ nanobelt arrays were also measured, but they are not worth reporting because emission currents are too low and unstable. It may be attributed to instability of the materials when electrons are emitted at applied field.

3.3. Electric Transport Properties of Individual 3R-TaSe$_2$ Nanobelt

To further investigate the electrical transport mechanism, the dc conductance of a single nanobelt under different temperatures was measured on the FET device (its SEM image is shown in Figure 4(a) without applying a gate voltage). Figure 4(b) presents the typical temperature-dependence *I–V* curves of the device in the temperature range of 8–300 K. It can be seen that the current increases with rising temperature (which is consistent with a typical semiconductor). A resistance versus temperature (*R–T*) curve (Fig. 4(c)) demonstrates the typical semiconductor behavior, though *R* abruptly bumps up at 160 K and 90 K. The bumps are likely attributed to CDW phase transitions of 3R-TaSe$_2$.[17] 3R-TaSe$_2$ bulk materials have been found to reveal metallicity,[15] but here the individual nanobelt shows a semiconducting behavior. This is probably ascribed to the nonstoichiometric chemical composition of the nanobelt, resulting in change of a metal to a semiconductor. We attempted to explain the semiconducting behavior by the small polaron theory (Mott proposed a conduction model of the optical phonon assisted hopping of small polarons between the localized states in
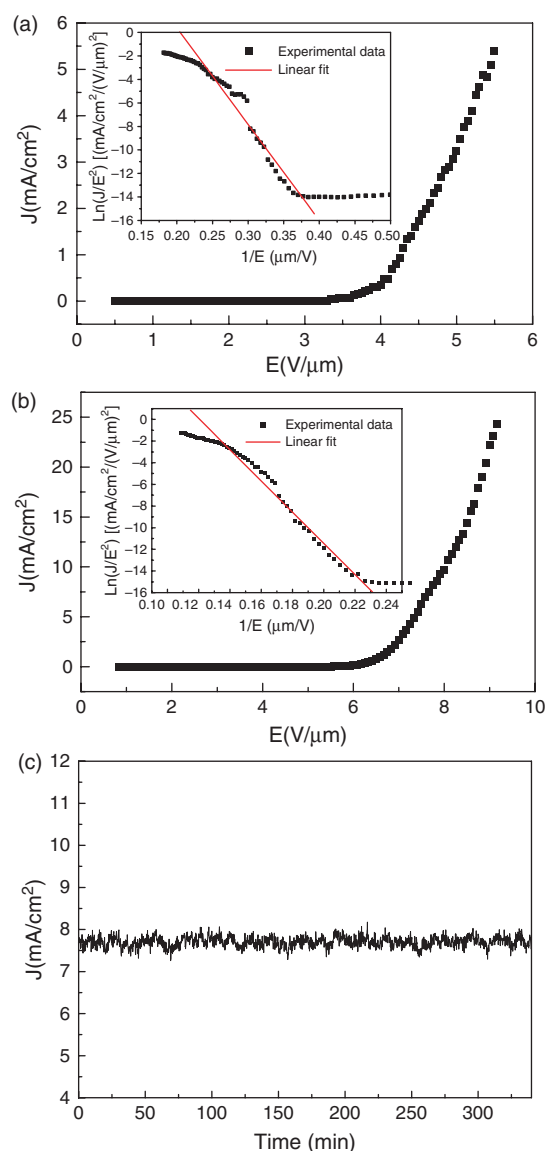
Fig. 3. Current density-applied field curves and the corresponding Fowler-Nordheim plots (insets) of aligned TaSe$_2$ nanobelts at an anode–cathode separation of (a) 200 μm, and (b) 120 μm. (c) Emission current density-time plot of the aligned TaSe$_2$ nanobelts at an applied field of 7.7 V/μm.

transition-metal oxides),[48, 49] and calculated the activation energies (ΔE) at 300–125 K, 155–30 K, and 30–8 K as 0.042, 0.064, and 0.0015 eV, respectively. However, the case was found to be better described by the variable-range hopping model proposed by Davis and Mott. According to an equation: $\sigma = \sigma_0 \exp[-(T_0/T)^{1/4}]$ (where σ_0 and T_0 are constants),[50] the curve in Figure 4(d) is well fitted at 300–120 K, and 120–8 K ranges. Therefore, as the temperature decreases, the optical phonons do not have enough energy to assist hopping so that their contribution to conduction process decreases, whereas the hopping process assisted by single acoustic phonons dominates.

5

RESEARCH ARTICLE
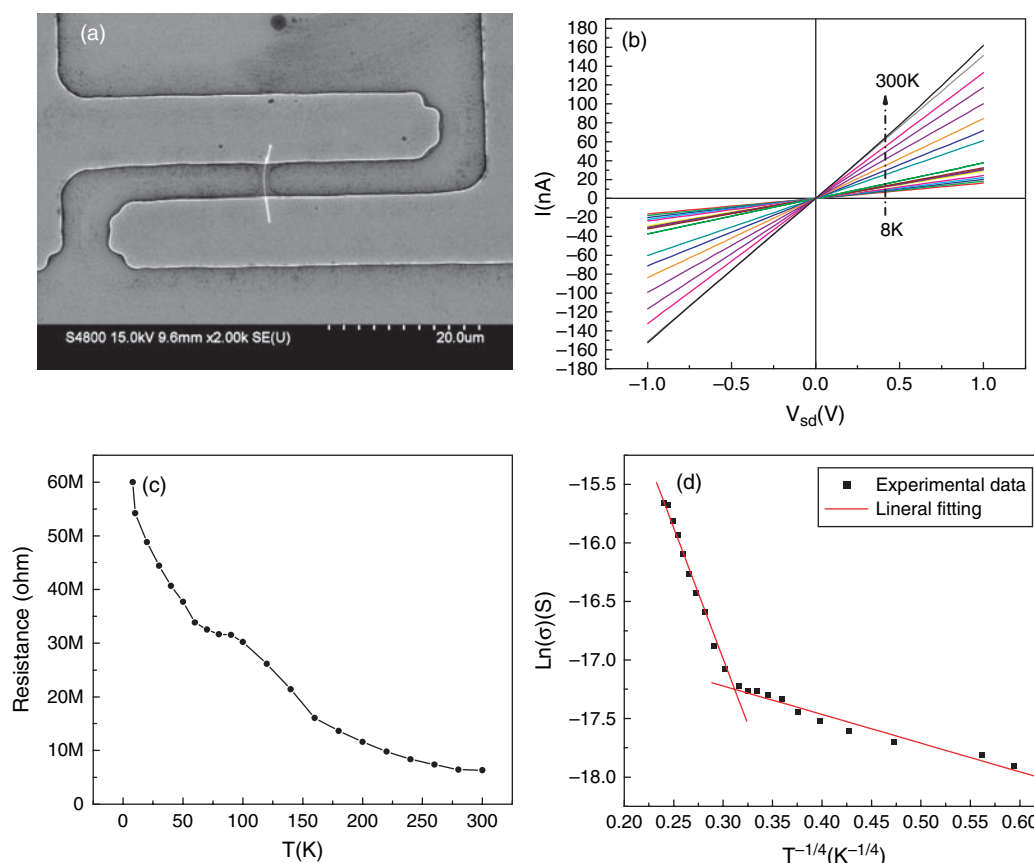
Fig. 4. (a) SEM image of a field-effect-transistor device designed for measuring electrical transport in a TaSe$_2$ nanobelt. (b) *I–V* curves recorded on a single nanobelt within the temperature range of 8–300 K. (c) Plot of *R* versus *T*. (d) σ versus $T^{-1/4}$. The solid line is the fit to the variable-range hopping model.

4. CONCLUSIONS

In summary, high-quality 3R-TaSe$_2$ nanobelt arrays have been fabricated using a facile two-step method. Field emission measurements show that the nanobelt arrays are high-performance field emitters. Electric transport measurement of the individual TaSe$_2$ nanobelt shows that the nanobelts are semiconducting materials. They are envisaged to find useful applications in vacuum microelectronic.[51]

References and Notes

1. M. G. Bawendi, M. L. Steigerwald, and L. E. Brus, *Annu. Rev. Phys. Chem.* 41, 477 (**1990**).
2. A. P. Alivisatos, *Science* 271, 933 (**1996**).
3. H. Weller, *Angew. Chem. Int. Ed.* 32, 41 (**1993**).
4. Y. Xia, P. Yang, Y. Sun, Y. Wu, B. Mayers, B. Gates, Y. Yin, F. Kim, and H. Yan, *Adv. Mater.* 15, 353 (**2003**).
5. N. I. Kovtyukhova and T. E. Mallouk, *Chem. Eur. J.* 8, 4355 (**2002**).
6. D. V. Bavykin, J. M. Friedrich, and F. C. Walsh, *Adv. Mater.* 18, 2807 (**2006**).
7. H. A. Nilsson, P. Caroff, C. Thelander, E. Lind, O. Karlstrom, and L. E. Wernersson, *Appl. Phys. Lett.* 96, 153505 (**2010**).
8. O. Knopfmacher, A. Tarasov, W. Y. Fu, M. Wipf, B. Niesen, M. Calame, and C. Schonenberger, *Nano Lett.* 10, 2268 (**2010**).
9. Y. Yang, J. J. Qi, W. Guo, Y. S. Gu, Y. H. Huang, and Y. Zhang, *Phys. Chem. Chem. Phys.* 12, 12415 (**2010**).
10. L. Li, X. S. Fang, T. Y. Zhai, M. Y. Liao, U. K. Gautam, X. C. Wu, Y. Koide, Y. Bando, and D. Golberg, *Adv. Mater.* 22, 4151 (**2010**).
11. J. Zhou, N. S. Xu, S. D. Deng, J. Chen, J. C. She, and Z. L. Wang, *Adv. Mater.* 15, 1835 (**2003**).
12. Z. W. Pan, H. L. Lai, F. C. K. Au, X. F. Duan, W. Y. Zhou, W. S. Shi, N. Wang, C. S. Lee, N. B. Wong, S. T. Lee, and S. S. Xie, *Adv. Mater.* 12, 1186 (**2000**).
13. X. C. Wu, Y. R. Tao, Q. X. Gao, and Y. L. Zhang, *J. Mater. Chem.* 19, 3883 (**2009**).
14. C. Pettenkofer, W. Jaegermann, A. Schellenberger, E. Holub-Krappe, C. A. Papageorgopoulos, M. Kamaratos, and A. Papageorgopoulos, *Sold State Commun.* 84, 921 (**1992**).
15. W. Geertsma, C. Haas, R. Huisman, and F. Jellinek, *Solid State Commun.* 10, 75 (**1972**).
16. T. Shimada, H. Nishikawa, A. Koma, Y. Furukawa, E. Arakawa, K. Takeshita, and T. Matsushita, *Surf. Sci.* 369, 379 (**1996**).
17. J. A.Wilson, F. J. Di Salvo, and S. Mahajan, *Adv. Phys.* 50, 1171 (**2001**).
18. R. K. Quinn, R. Simmons, and J. J. Banewicz, *J. Phys. Chem.* 70, 230 (**1966**).
19. Y. C. Jean and F. J. Disalvo, *Mol. Cryst. & Liq. Cryst.* 81, 867 (**1982**).

20. A. J. Patel, M. K. Bhayani, and A. R. Jani, *Chalcogenide Lett.* 6, 491 (**2009**).

21. T. Toshima and S. Tanda, *Physica C* 426–431, 426 (**2003**).

22. T. Toshima, K. Inagaki, N. Hatakenaka, and S. Tanda, *J. Phys. Soc. Jap.* 75, 024706 (**2006**).

23. M. Kars, A. Gomez-Herrero, A. Rebbah, and L. C. Otero-Diaz, *Mater. Res. Bull.* 44, 1601 (**2009**).

24. S. Tanda, T. Tsuneta, Y. Okajima, K. Inagaki, K. Yamaya, and N. Hatakenaka, *Nature* 417, 397 (**2002**).

25. Y. S. Hor, Z. L. Xiao, U. Welp, Y. Ito, J. F. Mitchell, R. E. Cook, W. K. Kwok, and G. W. Crabtree, *Nano Lett.* 5, 397 (**2005**).

26. Y. S. Hor, U. Welp, Y. Ito, Z. L. Xiao, U. Patel, J. F. Mitchell, W. K. Kwok, and G. W. Crabtree, *Appl. Phys. Lett.* 87, 142506 (**2005**).

27. T. Matsuura, M. Yamanaka, N. Hatakenaka, K. Matsuyama, and S. Tanda, *J. Cryst. Growth* 297,157 (**2006**).

28. W. Z. Wang, B. Q. Zeng, J. Yang, B. Poudel, J. Y. Huang, M. J. Naughton, and Z. F. Ren, *Adv. Mater.* 18, 3275 (**2006**).

29. J. D. Carey, *J. Nanosci. Nanotechnol.* 9, 6538 (**2009**).

30. T. Ghoshal, S. Biswas, S. Kar, and S. K. De, *J. Nanosci. Nanotechnol.* 9, 5586 (**2009**).

31. K. S. Park, Y. J. Choi, M. W. Ahn, D. W. Kim, Y. M. Sung, J. G. Park, and K. J. Choi, *J. Nanosci. Nanotechnol.* 9, 4328 (**2009**).

32. K. Huo, J. Fu, H. Ni, Y. Hu, G. Qian, P. K. Chu, and Z. Hu, *J. Nanosci. Nanotechnol.* 9, 3848 (**2009**).

33. Y. Li and H. W. Cheng, *J. Nanosci. Nanotechnol.* 9, 3301 (**2009**).

34. K. F. Huo, X. M. Zhang, J. J. Fu, G. X. Qian, Y. C. Xin, B. Q. Zhu, H. W. Ni, and P. K. Chu, *J. Nanosci. Nanotechnol.* 9, 3341 (**2009**).

35. G. X. Qian, K. F. Huo, J. J. Fu, and P. K. Chu, *J. Nanosci. Nanotechnol.* 9, 3347 (**2009**).

36. K. Y. Chun, S. I. Jung, H. Y. Choi, J. U. Kim, and C. J. Lee, *J. Nanosci. Nanotechnol.* 9, 2148 (**2009**).

37. Q. Zou and A. Hatta, *J. Nanosci. Nanotechnol.* 9, 924 (**2009**).

38. Y. L. Zhang, X. C. Wu, Y. R. Tao, C. J. Mao, and J. J. Zhu, *Chem. Comm.* 2683 (**2008**).

39. X. C. Wu , Y. R. Tao, and Q. X. Gao, *Nano Res.* 2, 558 (**2009**).

40. T. Y. Zhai, X. S. Fang, L. Li, Y. Bando, and D. Golberg, *Nanoscale* 2, 168 (**2010**).

41. X. S. Fang, Y. Bando, U. K. Gautam, C. H. Ye, and D. Golberg, *J. Mater. Chem.* 18, 509 (**2008**).

42. X. C. Wu, J. M. Hong, Y. R. Tao, Y. Deng, and Q. X. Gao, *J. Nanosci. Nanotechnol.* 10, 6465 (**2010**).

43. Y. R. Tao, Q. X. Gao, X. F. Wang, X. C. Wu, C. J. Mao, and J. J. Zhu, *J. Nanosci. Nanotechnol.* 11, 3345 (**2011**).

44. J. W. Gadzuk and E. W. Plummer, *Rev. Mod. Phys.* 45, 487 (**1973**).

45. N. S. Xu, Y. Chen, S. Z. Deng, J. Chen, X. C. Ma, and E. G. Wang, *J. Phys. D: Appl. Phys.* 34, 1597 (**2001**).

46. C. H. Ye, Y. Bando, X. S. Fang, G. Z. Shen, and D. Golberg, *J. Phys. Chem. C*, 111, 12673 (**2007**).

47. L. Li, X. S. Fang, H. G. Chew, F. Zheng, T. H. Liew, X. J. Xu, Y. X. Zhang, S. S. Pan, G. H. Li, and L. D. Zhang, *Adv. Funct. Mater.* 18, 1080 (**2008**).

48. S. Shi, X. Xue, P. Feng, Y. Liu, H. Zhao, and T. Wang, *J. Cryst. Growth* 310, 462 (**2008**).

49. J. Park, E. Lee, K. W. Lee, and C. E. Lee, *Appl. Phys. Lett.* 89, 183114 (**2006**).

50. S. Sen and A. Ghosh, *J. Appl. Phys.* 86, 2078 (**1999**).

51. W. Kume, Y. Tomoda, M. Hanada, and J. Shirakashi, *J. Nanosci. Nanotechnol.* 10, 7239 (**2010**).

RESEARCH ARTICLE